Dynamic measurements of the nonlinear elastic parameter α in rock under varying conditions

Paul A. Johnson,[1,2] Bernard Zinszner,[3] Patrick Rasolofosaon,[3]
Frederic Cohen-Tenoudji,[4] and Koen Van Den Abeele[5]

Received 18 June 2002; revised 26 August 2003; accepted 3 November 2003; published 4 February 2004.

[1] Since the exhaustive work by Adams and Coker at the Carnegie Institute in the early 1900s and the work of F. Birch's group at Harvard University conducted in the 1940s–1950s, it has been well documented that the quasi-static stress-strain behavior of rock is nonlinear and hysteretic. Over the past 20 years, there has been an increasing body of evidence suggesting that rocks are highly elastically nonlinear and hysteretic in their dynamic stress-strain response as well, even at extremely small strain amplitudes that are typical of laboratory measurements. In this work we present a compendium of measurements of the nonlinear elastic parameter α extracted from longitudinal (Young's mode) and flexural-mode resonance experiments in eight different rock types under a variety of saturation and thermal conditions. The nonlinear modulus α represents a measure of the dynamic hysteresis in the wave pressure-strain behavior. We believe that hysteresis is the primary cause of nonclassical nonlinear dynamics in rock, just as it is responsible for elastic nonlinear behavior in quasi-static observations. In dynamics, α is proportional to the wave speed and modulus reduction as a function of wave strain amplitude due to the hysteresis, based on our current model. The rocks tested include pure quartz sandstone (Fontainebleau), two sandstones that contain clay and other secondary mineralization (Berea and Meule), marble (Asian White), chalk, and three limestones (St. Pantaleon, Estaillades, and Lavoux). The values of α range from $\sim$500 to >100,000, depending on the rock type, damage, and/or water saturation state. Damaged samples exhibit significantly larger α than intact samples (hysteresis increases with damage quantity), and water saturation has an enormous influence on α from 0 to 15–30% water saturation. *INDEX TERMS:* 5102 Physical Properties of Rocks: Acoustic properties; 5112 Physical Properties of Rocks: Microstructure; 5199 Physical Properties of Rocks: General or miscellaneous; 9810 General or Miscellaneous: New fields (not classifiable under other headings); *KEYWORDS:* elastic nonlinearity, nonlinear acoustics, nonlinear elastic parameter α

Citation: Johnson, P. A., B. Zinszner, P. Rasolofosaon, F. Cohen-Tenoudji, and K. Van Den Abeele (2004), Dynamic measurements of the nonlinear elastic parameter α in rock under varying conditions, *J. Geophys. Res.*, *109*, B02202, doi:10.1029/2002JB002038.

1. Introduction

[2] Numerous elastic wave measurements in diverse solids have established that rock, concrete, some metals, and damaged materials exhibit nonclassical, nonlinear behavior [e.g., *Adams and Coker*, 1906; *Pandit and Savage*, 1973; *Guyer and Johnson*, 1999; *Johnson*, 1999]. By nonclassical behavior, we mean that a perturbation expansion of the stress-strain relation, the classical, atomic-elastic approach used for anharmonicity by, e.g., *Landau and Lifschitz* [1986], does not quantitatively predict observations in rock and some other materials (also see the books on classical nonlinear acoustics by *Blackstock and Hamilton* [1998] and *Naugolnykh and Ostrovsky* [1998]). In dynamics, we say these materials exhibit nonclassical nonlinear fast dynamics (NNFD) in that their elastic nonlinearity exhibits unique "signatures" not present in materials that exhibit classical nonlinear wave dynamics. These signatures include specific scaling relations between driving strains and detected wave harmonics, resonance peak shift and change in specific dissipation [e.g., *Ostrovsky and Johnson*, 2001]. These materials are also known as nonlinear mesoscopic elastic (NME) materials because their elasticity is attributable to the ensemble elastic behavior within the "bond system" at scales that may be near molecular up to 10^{-6} m, at least [*Guyer and Johnson*, 1999; T. W. Darling et al., Simultaneous neutron scattering and quasi-static stress-strain measurements in rocks, submitted to *Geophysical Reserch*

[1]Los Alamos National Laboratory, Los Alamos, New Mexico, USA.
[2]Also at the Laboratoire Environnement et Développement, Université Paris VII, Paris, France.
[3]Institut Français du Pétrole Reuil, Malmaison, France.
[4]Laboratoire Universitaire Applications Physique, Université Paris VII, Paris, France.
[5]Interdisciplinary Research Center, Faculty of Science, Catholic University, Kortrijk, Belgium.

0148-0227/04/2002JB002038$09.00

Letters, 2003]. Here we illustrate a compendium of results obtained from dynamic resonance experiments for diverse rocks that are part of the NME class. Experiments were conducted in a variety of samples under a variety of conditions of water saturations, temperatures, and thermally induced "damage" state in order to understand the qualitative relations between the nonlinear parameter α, rock type, and physical state; α is the measure of the stress-strain hysteresis in the material, and therefore a fundamental quantifier of NNFD.

[3] In the following, we briefly describe the classical and nonclassical theory known as the Preisach-Mayergoyz (P-M) space model of nonlinear elasticity [*McCall and Guyer*, 1994] and illustrate predictions from this theory that can be compared with experiment. We then describe the experiments, present results and discussion, and conclude.

2. Theory

[4] The traditional theory of elastic wave propagation in a nonlinear acoustic or elastic medium is based on expressing the energy density as a function of the scalar invariants of the strain tensor [e.g., *Landau and Lifshitz*, 1986]. In one dimension, this leads to an equation of motion in the displacement field (u) of

$$\frac{\partial^2 u}{\partial t^2} = \frac{d}{dx}\left(c^2 \frac{du}{dx}\right), \tag{1}$$

where

$$c^2 = c_0^2\left[1 + \beta\left(\frac{du}{dx}\right) + \delta\left(\frac{du}{dx}\right)^2 + \ldots\right], \tag{2}$$

c is nonlinear elastic wave speed, c_0 is the linear elastic wave speed, du/dx is the strain ε, and β and δ are higher-order contributions to the nonlinear wave speed. Equation (2) tells us that as the stain amplitude increases, the wave speed (and modulus) will increase or decrease, depending on the sign and magnitude of β and δ. In resonance, the average of the strain field over one period is zero, and thus we can drop the term proportional to β and replace the term proportional to δ by its average. Rewriting equation (2) and dropping all terms in powers higher than 2 (we can do this because the strains are small), we have

$$\frac{c^2 - c_0^2}{c_0^2} \cong \frac{f^2 - f_0^2}{f_0^2} \cong \frac{2(f - f_0)}{f_0} \cong \frac{1}{2}\delta\varepsilon^2, \tag{3}$$

where f is the resonance frequency at increased strain level (nonlinear elastic) and f_0 is the lowest drive amplitude resonance frequency (presumed to be elastically linear). Equation (3) indicates that the change in wave speed squared (proportional to modulus) is proportional to the square of the strain amplitude by the nonlinear parameter δ. It has been demonstrated that the strain dependency in equation (3) is too large in rock by a factor of one in the exponent of the strain [e.g., *Guyer and Johnson*, 1999; *Van Den Abeele et al.*, 2000a, 2000b]. In order to describe the behavior observed in rock, *McCall and Guyer* [1994] developed the Preisach-Mayergoyz (P-M) Space model of elasticity that incorporates hysteresis into the stress-strain relationship, correctly predicting both quasi-static and dynamic nonlinear behavior in rock over certain strain intervals (order 10^{-6}). The details of this model for a Young's mode resonating bar can be found elsewhere [e.g., *Guyer et al.*, 1995].

[5] The fundamental premise underlying the model is that the macroscopic elastic behavior of rock is due to a large number of hysteretic mechanical "features" contained in the mechanically soft bonds between the mechanically hard grains of a rock. The actual physical origin of the hysteretic elastic units is not presumed, and in fact, remains a mystery and a topic of intense research [e.g., *Ostrovsky and Johnson*, 2001]. Many physical mechanisms have been proposed such as Hertz-Mindlin theory [e.g., *Johnson et al.*, 2000] and grain contact adhesion [*Sharma and Tuntuncu*, 1994]. No physical mechanism proposed explains all observations, however.

[6] In the model used here, the individual hysteretic mechanical units have equilibrium lengths that switch hysteretically between two configurations, open and closed. The ensemble behavior of the hysteretic units are tracked in what is known as P-M space that has axes of open and closing pressure. The density of the hysteretic units is tracked in P-M space as a function of wave pressure. The inverse modulus $1/K = -\partial\varepsilon/\partial P$ can be derived in terms of the wave strain and pressure, and the corresponding density of units in P-M space that are open and closed (here we are eliminating a tremendous amount of detail in the derivation of the P-M space approximation; please see *Guyer et al.* [1995] for more detail). Following the P-M space approximation through, the Young's modulus in a resonating bar can be written as

$$K(\varepsilon, \dot{\varepsilon}) = K_0\{1 - \alpha[\Delta\varepsilon + \varepsilon(t)\mathrm{sign}(\dot{\varepsilon})] + \ldots\}, \tag{4}$$

where K_0 is the linear modulus, $\Delta\varepsilon$ is the peak strain amplitude over a wave period, $\dot{\varepsilon} = \partial\varepsilon/\varepsilon t$ is the strain rate, and (sign $(\dot{\varepsilon})$ = 1 for $\dot{\varepsilon} > 0$) and (sign $(\dot{\varepsilon}) = -1$ for $\dot{\varepsilon} < 0$) [*Guyer et al.*, 1997; *Van Den Abeele et al.*, 1997]. The nonlinear coefficient α describes the quantity of hysteresis in the stress-strain relation, the equation of state (EOS). As α increases, so does the hysteresis in the EOS. Equation (4) indicates that as the wave strain amplitude increases, the modulus changes as well, this time however in a discontinuous manner (a butterfly-type behavior). The average modulus is found to always decrease with strain amplitude in rock (α, as introduced in equation (4), is positive). As a result we have, in the case of hysteresis being the dominant cause of nonlinearity, that the elements or features in the material contributing to the nonlinearity contained in the bond system, some hysteretic (nonclassical) and some not (classical), make a contribution to the motion of the displacement field that depends on the actual strain value, the strain derivatives and the strain amplitude in a typically nonanalytic manner. In the case of a strain field with one frequency present as in a resonance bar experiment, the hysteretic nonlinear term leads to a resonance frequency shift, which is proportional to the peak strain amplitude,

$$\frac{f(\Delta\varepsilon) - f_0}{f_0} = \frac{\Delta f(\Delta\varepsilon)}{f_0} \cong \alpha_f \Delta\varepsilon, \tag{5}$$

where f_0 is again the elastically linear resonance frequency (in practice, the resonance frequency of the lowest drive

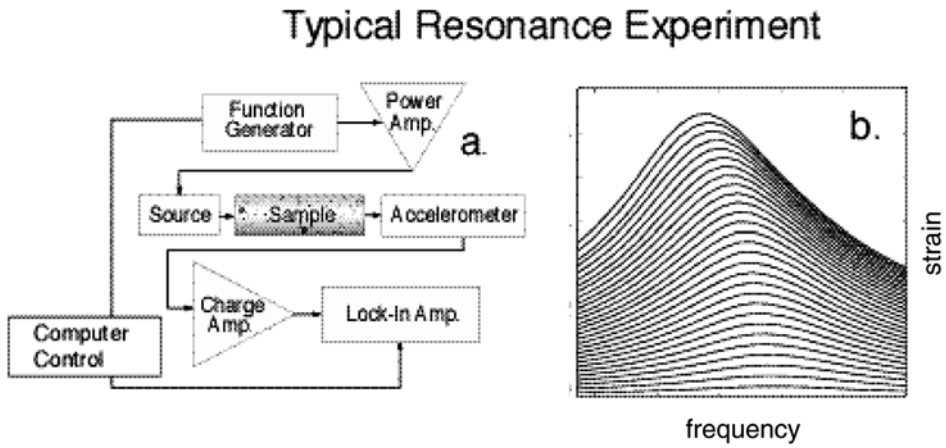

Figure 1. (a) Experimental configuration and (b) typical Young's mode resonance curves in a nonlinear mesoscopic elastic material. Time-averaged amplitude is plotted against the resonance frequency. By plotting the resonance peak versus the associated peak strains, one extracts α_f.

amplitude). In terms of the actual resonance bar experiment, one measures the peak resonance frequency as a function of the strain at progressively larger driving amplitudes, and fits these data to extract α.

[7] It can be shown that the change in nonlinear attenuation is proportional to α, meaning the attenuation is strain amplitude dependent as well. This relation, derived, for instance, by *Guyer et al.* [1999], is

$$\frac{1}{Q(\varepsilon)} - \frac{1}{Q_0} \cong \alpha_Q \Delta\varepsilon, \tag{6}$$

where $\Delta\varepsilon$ is the magnitude of the strain field again, $1/Q(\Delta\varepsilon)$ is the nonlinear attenuation as a function of the strain field, and $1/Q_0$ is the linear elastic attenuation. Thus the frequency shift and $1/Q$ are proportional to the magnitude of the strain field, with $\alpha_Q/\alpha_f = 0.3$ for materials where this relation has been calculated (e.g., P. A. Johnson and A. Sutin, Slow dynamics in diverse solids, submitted to *Physical Review B*, 2003). In the data presented in this paper, Q was not measured; however based on equation (8), α_Q can be estimated.

[8] Other models of hysteresis in the EOS exist for rock. The P-M space model is the only one to our knowledge that correctly predicts both quasi-static and dynamic elastic nonlinear behaviors in rock, and provides one the ability to predict dynamic from quasi-static behavior. Nonetheless, there are no underlying physics in the P-M space model as they are currently unknown.

3. Experiment

[9] Figure 1a illustrates a typical Young's mode resonance experiment where a bar of material is excited by a sinusoidal oscillation. The signal frequency is swept through the fundamental mode resonance peak while the time-average amplitude of the output signal is measured and recorded. The drive amplitude is increased; the frequency is again swept in the same manner for progressively increasing drive levels (for additional details, see *Johnson et al.* [1996], *Zinszner et al.* [1997], and *Van Den Abeele et al.* [2000b]). Figure 1b illustrates a typical result in an NME material. The difference between the resonance peak frequency ω (at a finite amplitude drive level) and f_0 (at the lowest (linear) drive level) is then determined from each successive frequency sweep, normalized to the linear resonance peak f_0, and plotted against the strain amplitude. The strain intervals where one can reliably apply the P-M space model are limited to a range from 10^{-6} to roughly 10^{-5} (see Figure A3). Ten rock samples were tested of eight rock types. For comparison and to be certain the system electrical and contact nonlinearities had no influence, three materials known to be elastically linear were tested: Plexiglas, PVC, and polycarbonate [e.g., *Johnson et al.*, 1996]. Table 1 displays information regarding the sample sizes, provenance, strength, permeability and mineralogy, in addition to sample sizes of the three elastically linear standards used for comparison.

[10] Details of each experiment are provided in sections 3.1–3.8.

3.1. Berea Sandstone

[11] During this experiment the sample was taken to 65°C in a vacuum oven, held there for 120 hours, taken to 100°C and held for ~24 hours, then taken to 120°C where the source and detector failed. The sample was removed from the vacuum and placed in water to be thermally shocked and saturated (Hirswald saturation [*Bourbié et al.*, 1986]), then dried. Reliable α_f were measured at 65°C, at 65°C after 120 hours, at 100°C twice in succession, immediately after thermal shock/full saturation, and during drying. A second group of water saturation experiments conducted by *Van Den Abeele et al.* [2002] were conducted for a parallelepiped-shaped sample of Berea sandstone using the fundamental flexural resonance. These results are compiled here as well. Note that the α obtained in this case is therefore for the flexural mode. Saturation levels were estimated by the change in weight as compared with the oven dry weight.

3.2. ASI Marble

[12] In this experiment, a marble sample (Asian White Marble, ASI) was measured at ambient conditions, taken to

Table 1. General Rock Properties[a]

Rock	Provenance	Dimensions, cm	Compressive Strength, MPa	Air Permeability, mdarcy	Description
ASI Marble	Turkey	38.4 × 2.5		≪1	rhombohedral, monocrystalline magnesium calcite
Estaillades Limestone	France	116 × 8		300	bioclastic limestone
Berea sandstone (a)	United States	48.7 × 5	32		fine-grained sandstone, 85% quartz, 8% feldspar, 2% smectite, 2% mica/illite, 1% kaolinite
Berea sandstone (b)	United States	25.5 × 2.6 × 0.95 rectangular parallelepiped	32		fine-grained sandstone, 85% quartz, 8% feldspar, 2% smectite, 2% mica/illite, 1% kaolinite
Meule Sandstone	France	107.6 × 5	35	180	fine-grained, argillaceous (illite, kaolinite) micaceous sandstone: 74% quartz, 21% feldspar, 2% smectite, 2% mica/illite, 1% kaolinite
Fontainebleau sandstone	France	39 × 4	>70	1200	Pure quartz sandstone
St. Pantaleon limestone	France	115.5 × 8		4000	Bioclastic limestone
Lavoux limestone	France	115 × 5	25		pelletoidal limestone, 99% calcite
Lavoux limestone	France	25.5 × 2.6 × 0.95 rectangular parallelepiped	25		pelletoidal limestone, 99% calcite
Chalk	France	63.8 × 9		4	pure calcite
PVC		120 × 10.5		0	
Plexiglas		34 × 4		0	
Polycarbonate		101.6 × 4		0	

[a]Sample information for the seven rocks and three elastic linear standards described in this paper (circular cylinder except as noted). Information is left blank where data do not exist.

200°C in a vacuum oven, submerged in water and thereby thermally shocked simultaneous to becoming saturated (Hirswald saturation), removed from the water bath, monitored just postshock then dried under room conditions. The α_f were determined before heating, at 200°C, just post saturation and at two times during drying.

3.3. Estaillades Limestone

[13] Four measurements were taken at ambient conditions. Water saturations at the time of the experiments were <5%.

3.4. Fontainebleau Sandstone

[14] Four measurements were made in a vacuum oven at 40°C over a period of days.

3.5. St. Pantaleon Limestone

[15] The sample was oven dried under vacuum conditions at ~40°C, saturated (Hirswald saturation), and then dried. Reliable measurements were obtained at the saturations indicated. Data were of very poor quality for the midrange saturation levels and were discarded. Saturation was estimated by the change in weight as compared with the oven dry weight.

3.6. Chalk

[16] The sample was oven dried, saturated, and then dried again. Measurements were made at the water saturations indicated. Saturation was estimated by the change in weight as compared with the oven dry weight.

3.7. Meule Sandstone

[17] The sample was oven dried under vacuum, saturated, and then dried. Measurements were made at many saturations. Saturation was estimated by the change in weight as compared with the oven dry weight.

3.8. Berea Sandstone and Lavoux Limestone Flexural-Mode Measurements

[18] The parallelepiped samples were oven dried under vacuum, saturated, and then dried. Measurements were made at many saturations. Saturation was estimated by the change in weight as compared with the oven dry weight. The measurements were obtained from flexural-mode resonance and therefore it is the flexural-mode α_f that is calculated. A comprehensive analysis of these data in the context of the influence of pore pressure on elastic nonlinearity was conducted by *Van Den Abeele et al.* [2002]. A description of how the flexural mode α_f is derived is also contained in this work.

4. Results

[19] Figure 2 shows the relation of the change in resonance frequency $\Delta f/f_0$ as a function of strain amplitude

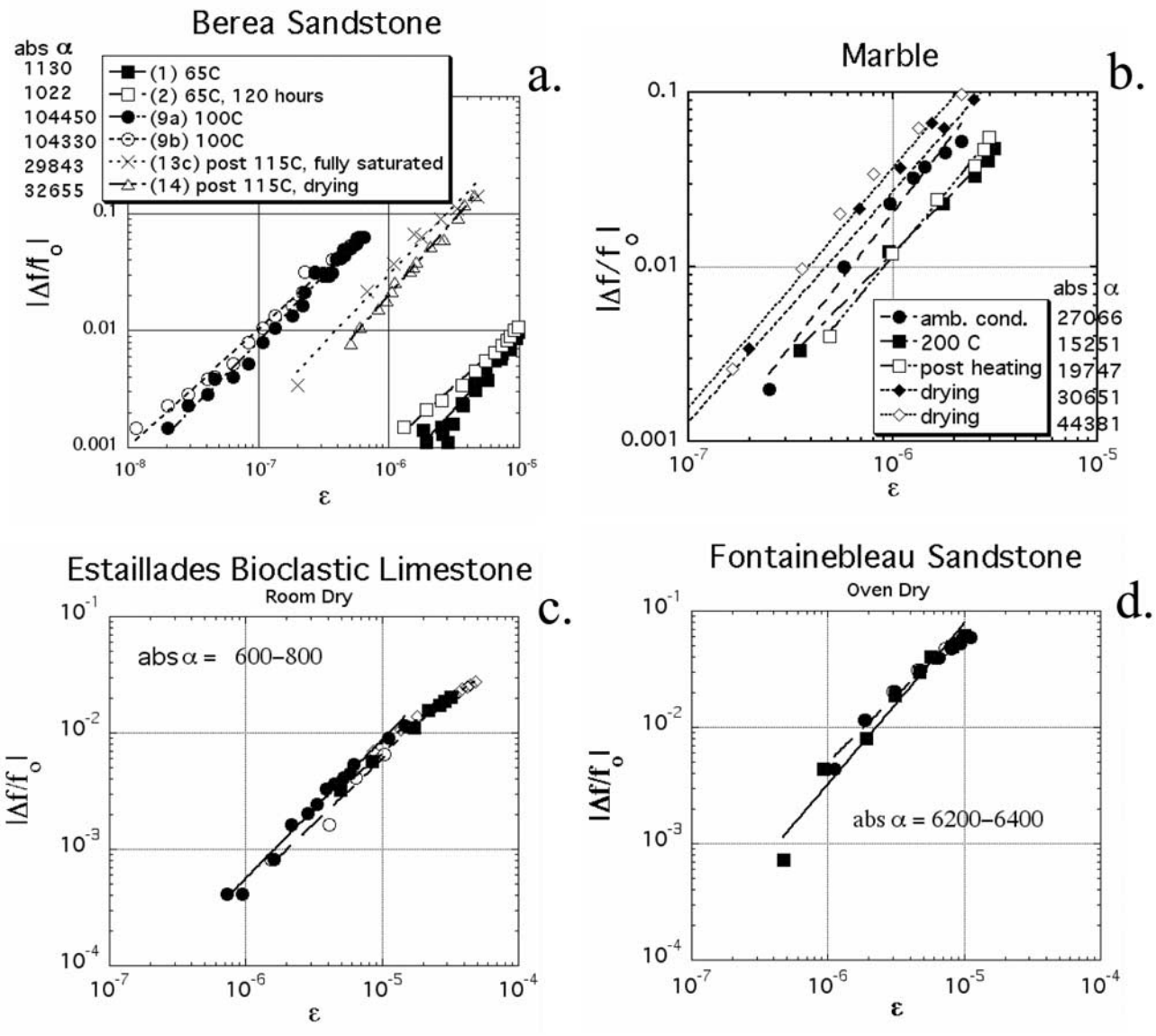

Figure 2. Change in frequency $|\Delta f/f_0|$ with strain amplitude $\varepsilon = \Delta\varepsilon$ in four materials under varying conditions as noted. The hysteretic nonlinear parameter α_f is shown for each sample under all conditions monitored. For the Berea sample (Figure 2a), the damage took place before the sample reached 100°C. In the case of the ASI marble (Figure 2b), the sample was taken out of the oven and placed in a water bath in order to shock it.

$\Delta\varepsilon$ for the samples of Berea sandstone (Figure 2a), ASI marble (Figure 2b), Estaillades limestone (Figure 2c), and Fontainebleau sandstone (Figure 2d). The estimated α_f are shown in Figure 2 for all conditions and are tabulated in Table 2. Figure 3 shows similar results for the saturation tests conducted on the samples of St. Pantaleon limestone (Figure 3a), chalk (Figure 3b), and Meule sandstone (Figure 3c). Again, α_f are shown in Figure 3 and later tabulated in Table 2 together with linear properties. Note the huge variation of α_f that correspond to different damage/saturation states.

[20] Figure 4 shows the results from measurements in three standards up to strains far greater than those in the rock samples ($>10^{-4}$ in the case of the polycarbonate), indicating that the system nonlinearities are negligible. Figure 5 shows α_f as a function of saturation for the Meule sandstone and the chalk samples. Figures 6a–6f shows the relation between velocity c^2, proportional to Young's modulus, with the change in α_f for each rock sample. Figure 6f shows all data together. Note that except for the ASI marble, the change in α_f is 2–3 orders of magnitude while the change in modulus is less than an order of magnitude for the various physical states.

5. Discussion

[21] The slopes of the change in frequency with strain are universally one as the P-M space theory predicts. This is indeed gratifying considering the huge differences in chemical and physical makeup of these materials. It is important to note that the correct selection of the linear resonance frequency is extremely important and one must be careful in doing so. Appendix A describes why.

Table 2. Rock Physical Conditions, Linear and Nonlinear Parameters

Rock Identification	Conditions	c^2, $(m/s)^2$	α_f
St. Pantaleon Bioclastic Limestone	~1% water saturation	7.8967e + 06	765
	67% water saturation	6.3981e + 06	2588
	74% water saturation	6.2934e + 06	2720
	93% water saturation	6.0410e + 06	2770
	97% water saturation	6.0410e + 06	2880
	100% water saturation	6.0410e + 06	3160
Estaillades Bioclastic Limestone	room dry (<5% water saturation)	8.0243e + 06	600–800
ASI Marble	<5% water saturation	9.0180e + 06	27066
	200°C, dry	6.7288e + 06	15251
	post-200°C, ~100% water saturation		19747
	post-200°C, drying, saturation unknown	6.6049e + 06	30651
	post-200°C, 40°C, <1% water saturation	2.5313e + 06	44381
Fontainebleau sandstone	<1%	6.3e + 03	6200–6400
Meule Sandstone	1% water saturation	4.07e + 06	2920
	3% water saturation	3.69e + 06	2570
	4% water saturation	3.66e + 06	2580
	6% water saturation	2.67e + 06	3815
	16% water saturation	1.76e + 06	10929
	27% water saturation	1.44e + 06	13709
	40% water saturation	1.41e + 06	8167
	30% water saturation	1.28e + 06	7688
	53% water saturation	1.40e + 06	9843
	69% water saturation	1.35e + 06	8303
	80% water saturation	1.35e + 06	9430
	83% water saturation	1.36e + 06	8087
	88% water saturation	1.35e + 06	8425
	95% water saturation	1.35e + 06	6864
	98% water saturation	1.49e + 06	6046
Berea Sandstone (cylinder)	65°C, $\ll$1% water saturation	3.7830e + 06	1130
	65°C, $\lll$1% water saturation	3.7986e + 06	1022
	115°C, $\lll$1% water saturation	3.4522e + 06	104450
	115°C, $\lll$1% water saturation	3.4336e + 06	104330
	thermally shocked, ~100% water saturation	1.3202e + 06	29843
	thermally shocked, drying, saturation unknown	3.8927e + 06	32655
Rock Identification	Conditions	c^2 $(m/s)^2$	Flexural-Mode α
Berea Sandstone (parallelepiped)	3.9% water saturation	3.7493e + 06	7012
	4.7% water saturation	3.6134e + 06	7424
	5.1% water saturation	3.7137e + 06	7722
	6.4% water saturation	3.1453e + 06	7622
	7.2% water saturation	2.9929e + 06	7927
	7.9% water saturation	2.8483e + 06	8276
	11.1% water saturation	2.3372e + 06	7720
	12.0% water saturation	2.2976e + 06	7172
	13.3% water saturation	2.1907e + 06	7234
	14.5% water saturation	2.1092e + 06	7673
	16.6% water saturation	1.8942e + 06	6779
	17.1% water saturation	1.8915e + 06	6617
	19.5% water saturation	1.8187e + 06	7096
	20.1% water saturation	1.8646e + 06	6628
	22.4% water saturation	1.7742e + 06	6640
	24.2% water saturation	1.8193e + 06	6433
	27.4% water saturation	1.7596e + 06	6492
	32.1% water saturation	1.7964e + 06	6097
	35.4% water saturation	1.7316e + 06	6023
	51.1% water saturation	1.6921e + 06	5681
	52.6% water saturation	1.7724e + 06	6201
	53.0% water saturation	1.7575e + 06	6053
	53.7% water saturation	1.6892e + 06	5682
	56.7% water saturation	1.6786e + 06	5609
	60.6% water saturation	1.6752e + 06	5795
Lavoux Limestone(parallelepiped)	0.10000% water saturation	8.3500e + 06	2888.8
	1.0000% water saturation	8.2800e + 06	2877.3
	1.5000% water saturation	8.2100e + 06	2865.8
	5.0000% water saturation	7.6700e + 06	2769.2
	8.0000% water saturation	7.5500e + 06	2748.5
	20.000% water saturation	7.1900e + 06	2681.8
	24.000% water saturation	7.1400e + 06	2672.6
	31.000% water saturation	7.0400e + 06	2654.2
	45.000% water saturation	6.8900e + 06	2624.3
	50.000% water saturation	6.7300e + 06	2594.4
	64.000% water saturation	6.6000e + 06	2569.1
	73.000% water saturation	6.5100e + 06	2550.7
	80.000% water saturation	6.5400e + 06	2556.4
	98.000% water saturation	6.8400e + 06	2615.1

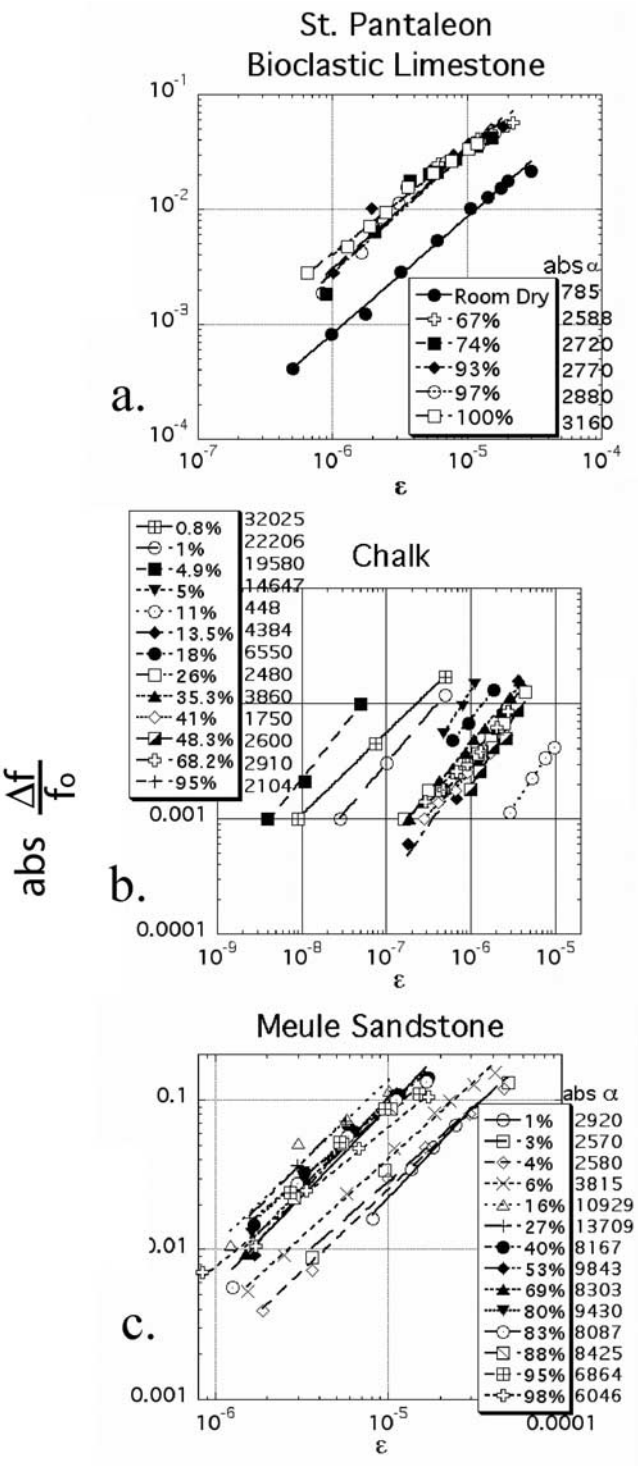

Figure 3. Change in frequency $|\Delta f/f_o|$ with strain amplitude $\varepsilon = \Delta\varepsilon$ in three materials under varying water saturation conditions as noted. The hysteretic nonlinear parameter α_f is shown for each sample under all conditions monitored.

5.1. Thermal Shock-Induced Damage

[22] The results shown in Figure 2 give an idea of the range of the α_f under mostly dry conditions. The huge change in α_f between 65 and 100°C in Berea sandstone could be due in part to decreasing water saturation (see below) but more importantly, to damage that occurred while the sample was at or above 100°C. The value of α_f increases by an order of magnitude with the introduction of thermal damage. Note that it is well established empirically that hysteresis and therefore α_f increases with damage quantity [e.g., *Johnson*, 1999; *Van Den Abeele et al.*, 2000b]. The sample did not return to its original state after heating as seen in later tests not shown, and we verified that thermal damage had taken place by qualitative visual inspection after the experiment. The ASI marble (Figure 2b) exhibits different behavior than the sandstone during heating in that the ambient α_f is smaller than that measured at 200°C, and as the sample dries after saturation, α_f becomes larger. In addition, the change in α_f is comparable to that in the linear modulus. The ASI marble appears to have an ability to heal itself in some manner during the heating and shock procedure. Detailed inspections for damage the samples using such techniques as using photomicrographs and other methods were not conducted. This certainly would have been of some value, but at the same time, it is known that the damage scale that induces elastic nonlinear behavior can apparently range from near atomic to 10^{-3} m at least [e.g., *Ten Cate et al.*, 2000], and therefore such inspections are of limited value. In fact, the quantitative relation between damage and the nonlinear coefficient remains a central question in this domain of study, and is actively being pursued by several groups. This is to say, we do not know what the origin of the nonlinear behavior is. We only know that α is empirically correlated to damage (whatever that means) at all scales tested to date.

5.2. General Comments on Other Samples

[23] The sample of Estaillades limestone shown in Figure 2c has a relatively low range of α_f in the dry state compared with the other rocks. We submit that this is because the limestone has a relatively small amount of inherent microdamage/macrodamage compared to the other rocks. The result on dry St. Pantaleon limestone is very similar so this may be characteristic of limestones in general. Fontainebleau sandstone in particular is highly nonlinear in its natural, dry state, and this is due to the friability of the bond structure, we believe. Chalk is also very nonlinear under all saturation conditions as has been noted before [*Johnson et al.*, 1996], and we believe this is due to the Velcro-like nature of the microplanktonic fossil material that comprises the chalk [e.g., *Bourbié et al.*, 1986; *Lucet et al.*, 1991].

5.3. Effects of Water Saturation

[24] *Van Den Abeele et al.* [2002] conducted quantitative studies of the effect of contained moisture in several rock samples, including the same Meule sandstone and Lavoux limestone samples. Their studies show that at low water saturations, molecular layers of adsorbed fluids as well as capillary condensation significantly influence the dynamic and linear nonlinear behavior due to the induced internal molecular forces. They observed a significant increase in the nonlinear response in several rocks in the saturation range of 1–20% especially in rocks containing small pore systems such as limestone. This is a result of an increased fluid-solid interaction upon wetting causing the material to expand and soften. Simultaneously,

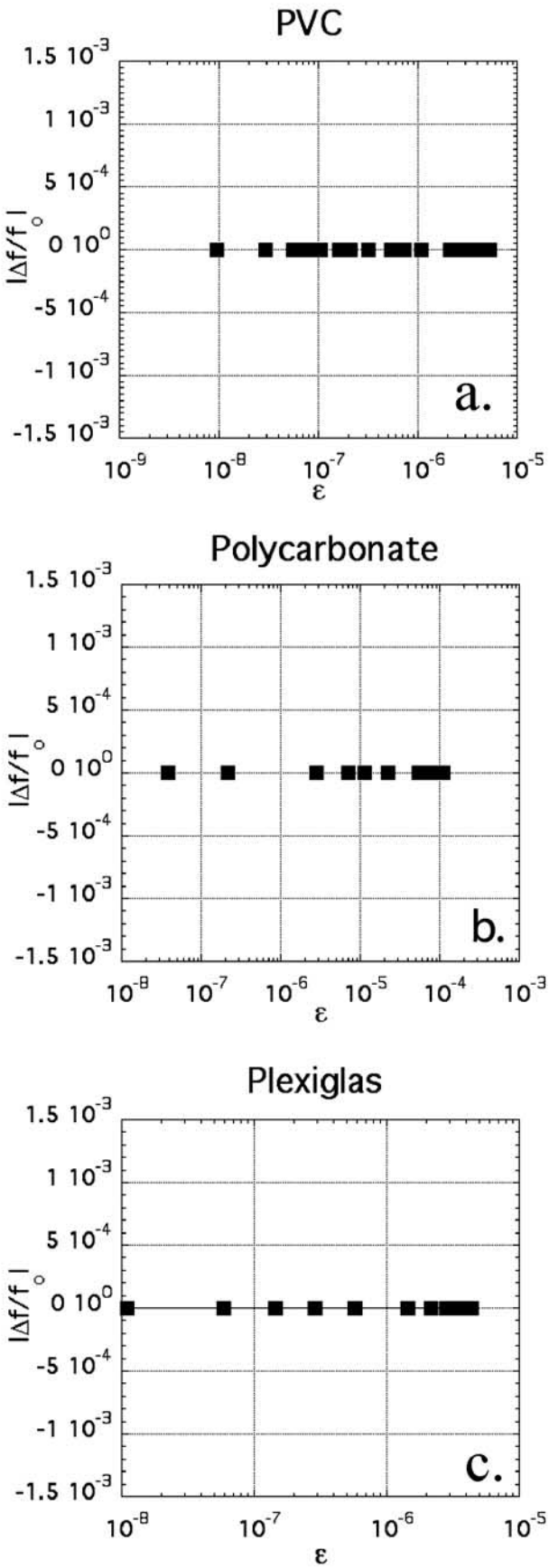

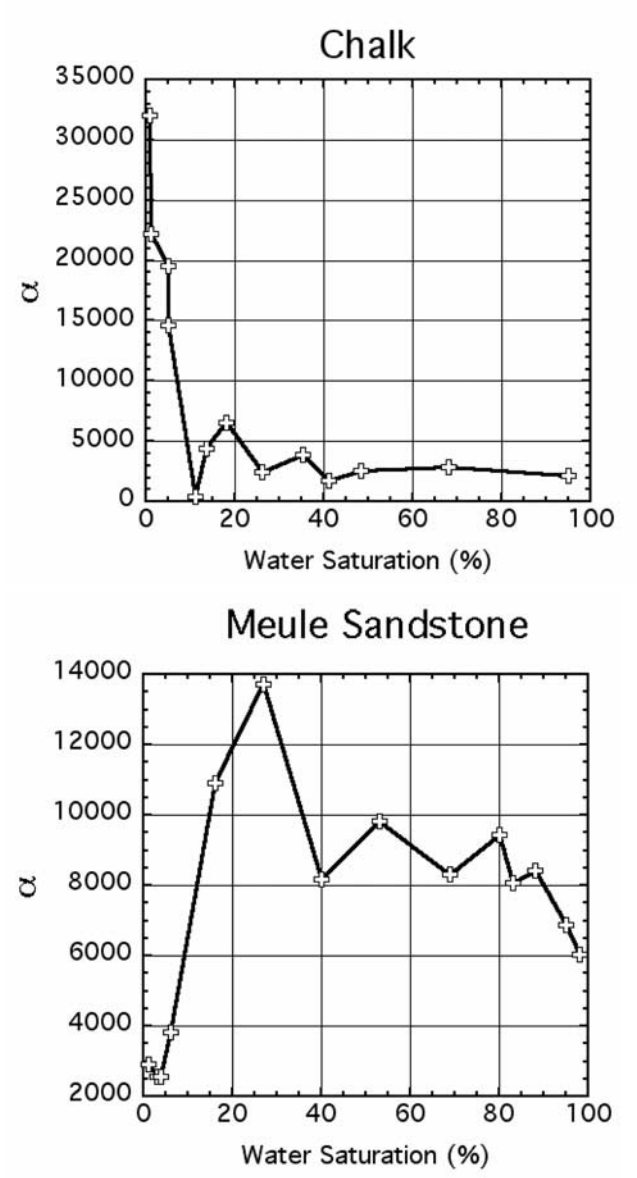

Figure 5. The α_f as function of water saturation in two rock types.

the microscopic and mesoscopic hysteretic entities that are, in ensemble, the origin of nonlinear response, are progressively activated at different pressures as a function of low water saturation. As a consequence of the moisture-induced forces, the number of active hysteretic units increases with saturation. The fact that the nonlinear response increases with water saturation especially in the low saturation range, implies that the presence of moisture plays a major role in the nonlinear mechanism(s), or in the activation of that (those) mechanism(s).

Figure 4. Change in frequency $|\Delta f/f_o|$ with strain amplitude $\varepsilon = \Delta\varepsilon$ in three "linear" elastic standards used to compare with results obtained in the rocks. The $\alpha_f = 0$ in each case.

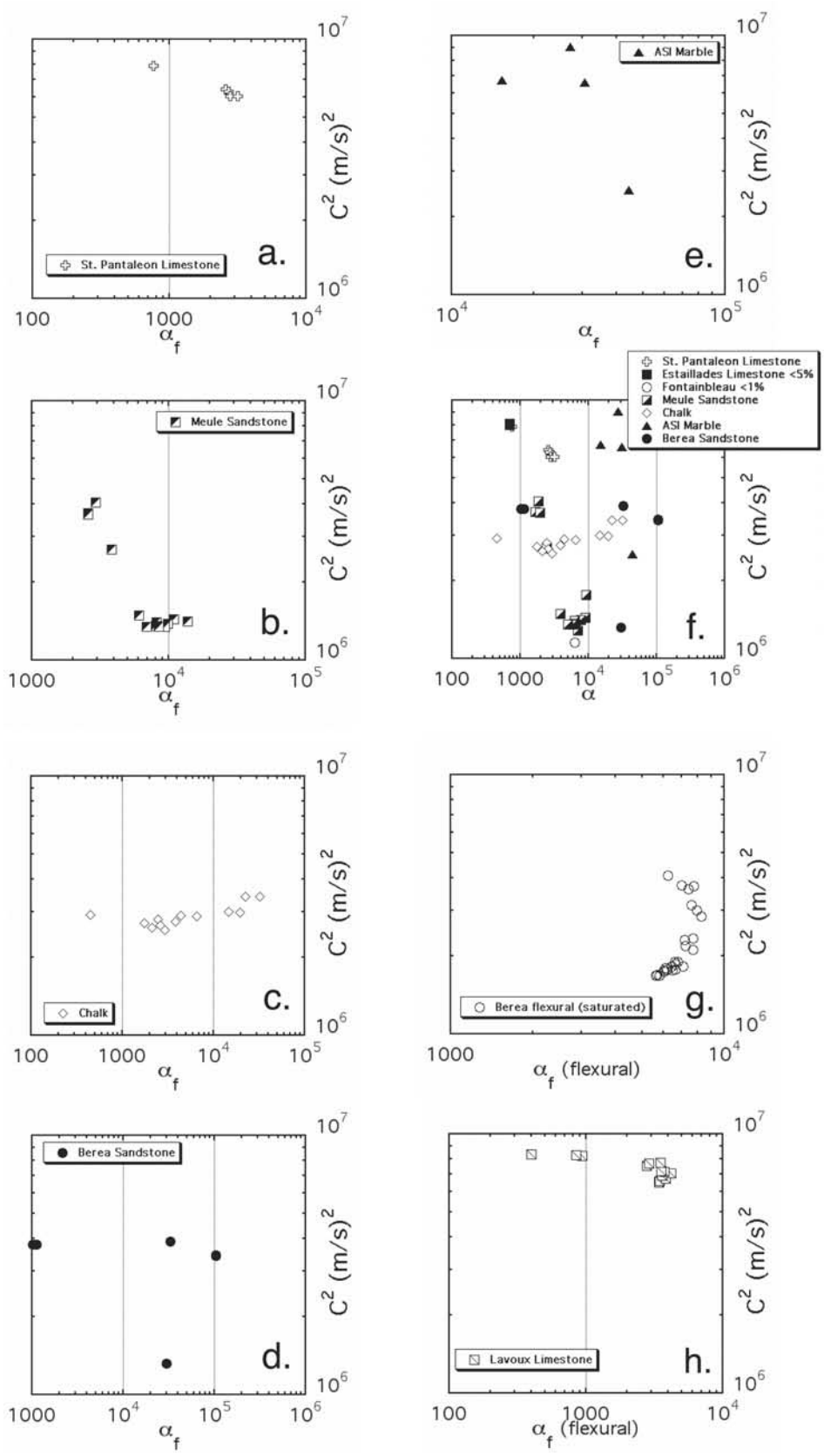

Figure 6. (a)–(e) Velocity squared, proportional to Young's modulus, versus α_f for each of the rock samples (excluding Fontainebleau sandstone and Estaillade limestone) under all conditions tested. (f) Combined data. (g)–(h) Flexural data from *Van Den Abeele et al.* [2002].

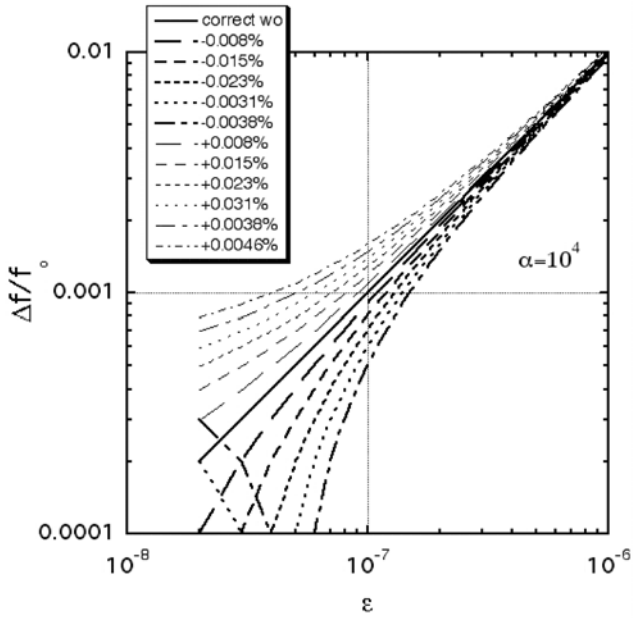

Figure A1. Systematic errors in normalized resonance angular frequency shift $|\Delta f/f_0|$ as a result of errors due to incorrect selection of the linear frequency ω_0. Horizontal axis is the strain amplitude $\Delta\varepsilon$ of each resonance peak. The correct f_0 for a nonclassical model is shown by the solid line, where the nonlinear parameter $\alpha = 10^4$. The percent error up to ±0.0006 is shown. Clearly, even very small errors in f_0 lead to significant errors in the $|\Delta f/f_0|$ versus $\Delta\varepsilon$, particularly at small strain levels.

[25] At higher levels of saturation, capillary condensation takes place. Capillary condensation commences when the molecular adsorbed water layers in the finest pores abruptly alter to a more stable arrangement, due to surface tension, by forming a meniscus between the liquid water and gas phase. As one may expect, this sudden transition does not occur uniformly over the entire sample. It is highly dependent on the range of pore dimensions inherent to rocks. Since the microscopic capillary pressure in absence of external loads is always positive, it exerts a tensile loading. The sparse data set available for the St. Pantaleon limestone fits the above interpretation as well.

[26] The chalk sample exhibits entirely different behavior at low water saturations. The nonlinear response is enormous until between 5 and 10% water saturation, where it begins to resemble the behavior of other rocks. We do not know why the sample displays such behavior but chalk is well known to display peculiar mechanical behavior [e.g., *Bourbié et al.*, 1986; *Risnes and Flaageng*, 1999].

6. Conclusions

[27] In this article we present the longitudinal-mode hysteretic nonlinear parameter α_f for eight different rock types and two for the flexural-mode α_f. Rock types included are sandstones, limestones, marble, and chalk under a variety of damage and water saturation conditions. The range of α_f is several hundred to tens of thousand depending on physical state. Unfortunately, some of the work presented here, in particular for the thermal shock measurements is qualitative because comparisons could not be made to other measures of damage. On the other hand, the experiments conducted under controlled saturation conditions are truly quantitative. We hope that this work will spur further work into exploring and categorizing the nonlinear behavior of rock. We believe α will become a common identification physical parameter for rock, just as wave speed, Q, and modulus are today.

Appendix A: Errors in Calculation of the Nonlinear Parameter α

A1. Errors in Estimation of f_0

[28] Very small errors in the selection of ω_0 can lead to significant misfits in the frequency-strain relation. Figure A1 illustrates this effect in the frequency-strain scaling relation for a typical NME material nonlinear parameter $\alpha_f = 10^4$. Errors in f_0 can be due to too large drive frequency sampling in the time-averaged frequency response or broad resonance frequency peaks due to low

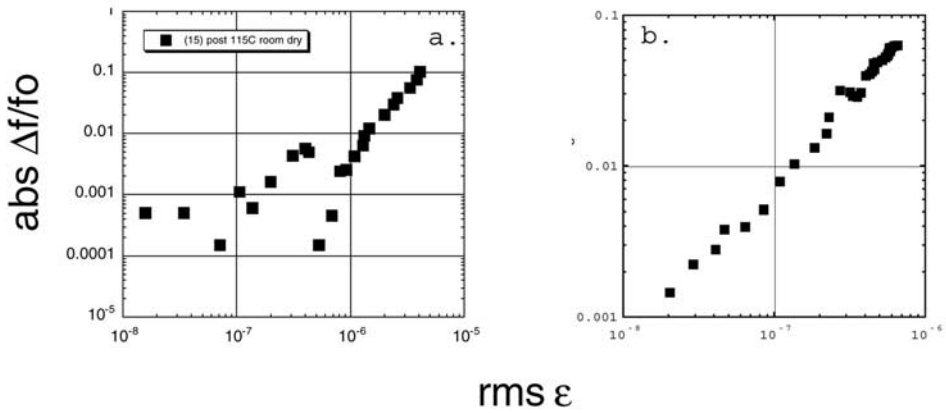

Figure A2. Selection errors in ω_0 that lead to errors in the dependence of frequency change $|\Delta\phi/\phi_0|$ to strain $\Delta\varepsilon$ from resonance experiments in Berea sandstone. (a) Selection of f_0 slightly low. (b) Selection of f_0 slightly high.

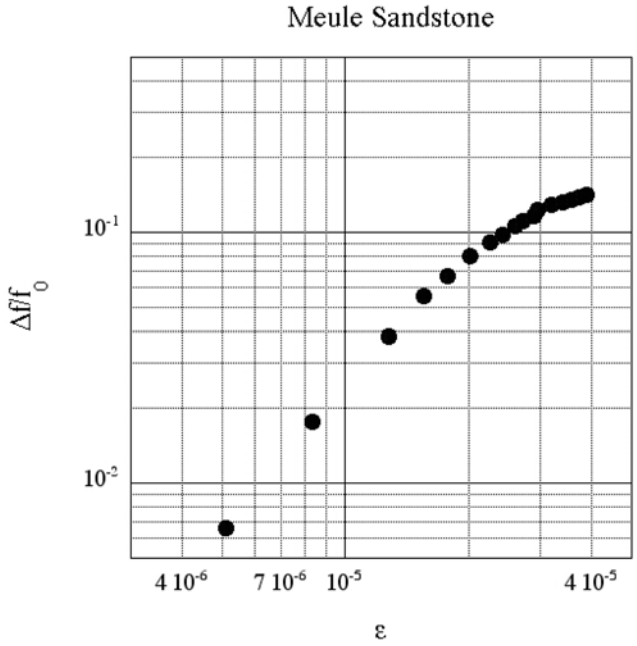

Figure A3. Example of higher-order nonlinear regime in Meule sandstone. At strains of approximately 2×10^{-5} the $|\Delta f/f_0|$ $-\Delta\varepsilon$ scaling relation begins to turn over. Strain amplitudes where this behavior is observed are not yet well understood.

values of Q, for instance, but more often to the effect of slow dynamics [e.g., *Ostrovsky and Johnson*, 2001; *Ten Cate et al.*, 2000]. In Figure A1, we create frequency-strain data and then estimate the effect of small errors in the choice of f_0. For instance, a 1 Hz error at a resonance frequency of 13 kHz is ±0.008% error. This error can easily appear in digital data where the drive frequency sampling may exceed 0.008%. The resulting slope fit is 0.84 and larger than 2, respectively. For an error of ±0.0031% (corresponding to a 4 Hz error in ω_0 at 13 kHz), the error in the fits becomes rapidly worse: as small as 0.7 and larger than 3, respectively, with severe influence on the small amplitude data. The details of the induced errors will vary with α; however, the general behavior will remain as illustrated in Figure A1.

[29] Figure A2a illustrates data taken from an experiment in Berea sandstone where f_0 was unintentionally chosen lower than the actual value. It is clear that a poor choice of ω_0 on the low-frequency side is not difficult to discern. On the other hand, a poor choice on the high-frequency side of ω_0 is more difficult. There is only a slight indication in the lowest amplitudes where an inflection point develops, as the error becomes larger. For example, Figure A2b illustrates one example. The inflection point occurring at just under $\varepsilon = 10^{-7}$ indicates that f_0 is too high. On the other hand, choosing f_0 too large introduces very little error.

A2. Slow Dynamics and Estimation of f_0

[30] The effects of slow dynamics on the resonance-frequency strain scaling relation are several. The most obvious is that a sample must be in its equilibrium rest state before a resonance experiment begins. That is to say, the sample must remain undisturbed for at least 10^3 s after a previous excitation. Otherwise, the modulus and therefore the linear resonance frequency f_0 will always be less than the actual equilibrium value, leading to influence on data as described in the previous figures. The effect will depend on the intensity of the slow dynamical response of a sample, and the equilibration recovery time. Changes of frequency of order of those shown in Figure A2 are not uncommon with relaxations of 10^3 s. On the other hand, this is a relatively easy effect to detect because it decreases resonance frequency, just as described earlier. In study of several hundred data sets for a large number of materials, we observe the effect of especially slow dynamics to be significant.

A3. Higher-Order Nonlinear Regime

[31] Figure A3. shows a result taken on Meule sandstone where the normalized frequency changes slope at larger strain levels. The first-order predictions based on a uniform P-M space model of nonlinear elasticity are not valid at these higher dynamic strain levels. It is a region in dynamic strain as yet not well explored. In this paper, data taken at strains beyond this inflection point were not used in the analyses.

[32] **Acknowledgments.** Work was supported by the Office of Basic Energy Science of the U.S. Department of Energy operated by the University of California, by the Institut Français du Pétrole, and by CNRS, France, and by the Foundation for Scientific Research of Flanders, Belgium.

References

Adams, F. D., and E. G. Coker (1906), An investigation into the elastic constants of rocks, more especially with reference to cubic compressibility, *Carnegie Inst.*, *46*.

Blackstock, D., and M. Hamilton (Eds.) (1998), *Nonlinear Acoustics*, Academic, San Diego, Calif.

Bourbié, T., O. Coussy, and B. Zinszner (1986), *Acoustics of Porous Media*, Technic, Paris.

Guyer, R. A., and P. A. Johnson (1999), Nonlinear mesoscopic elasticity: Evidence of a new class of materials, *Phys. Today*, *52*, 30–35.

Guyer, R. A., K. R. McCall, P. A. Johnson, P. N. J. Rasolofosaon, and B. Zinszner (1995), Equation of state hysteresis and resonant bar measurements in rock, *Proc. U.S. Rock Mech. Symp.*, *35th*, 177–185.

Guyer, R. A., K. R. McCall, G. N. Boitnott, L. B. Hilbert Jr., and T. J. Plona (1997), Quantitative implementation of Preisach-Mayergoyz space to find static and dynamic elastic moduli in rock, *J. Geophys. Res.*, *102*, 5281–5293.

Guyer, R. A., P. A. Johnson, and J. N. TenCate (1999), Hysteresis and the dynamic elasticity of consolidated granular materials, *Phys. Rev. Lett.*, *82*, 3280–3283.

Johnson, D. L., H. A. Makse, N. Gland, and L. Swartz (2000), Nonlinear elasticity of granular media, *Physica B*, *279*, 134–138.

Johnson, P. A. (1999), The new wave in acoustic testing, *Mater. World*, *7*, 544–546.

Johnson, P. A., and P. N. J. Rasolofosaon (1996), Manifestation of nonlinear elasticity in rock: Convincing evidence over large frequency and strain intervals from laboratory studies, *Nonlinear Processes Geophys.*, *3*, 77–88.

Johnson, P. A., B. Zinszner, and P. N. J. Rasolofosaon (1996), Resonance and nonlinear elastic phenomena in rock, *J. Geophys. Res.*, *101*, 11,553–11,564.

Landau, L. D., and E. M. Lifschitz (1986), *Theory of Elasticity*, 3rd rev, Engl. ed., Pergamon, New York.

Lucet, N., P. N. J. Rasolofosaon, and B. Zinszner (1991), Sonic properties of rock under confining pressure using the resonant bar technique, *J. Acoust. Soc. Am.*, *89*, 980–990.

McCall, K. R., and R. A. Guyer (1994), Equation of state and wave propagation in hysteretic nonlinear elastic material, *J. Geophys. Res.*, *99*, 23,887–23,897.

Naugolnykh, K., and L. Ostrovsky (1998), *Nonlinear Wave Processes in Acoustics*, Cambridge Univ. Press, New York.

Ostrovsky, L., and P. A. Johnson (2001), Dynamic nonlinear elasticity in geomaterials, *Riv. Nuovo Cimento Ital. Phys. Soc.*, *24*, 1–46.

Pandit, B., and J. C. Savage (1973), Experimental test of Lomnitz's theory of internal friction in rocks, *J. Geophys. Res.*, *78*, 6097–6099.

Risnes, R., and O. Flaageng (1999), Mechanical properties of chalk with emphasis on chalk-fluid interactions and micromechanical aspects, *Oil Gas Sci. Technol.*, *54*, 751–758.

Sharma, M. M., and A. Tuntuncu (1994), Grain contact adhesion hysteresis—A mechanism for attenuation of seismic waves, *Geophys. Res. Lett.*, *21*, 2323–2326.

Ten Cate, J., E. Smith, and R. Guyer (2000), Universal slow dynamics in granular solids, *Phys. Rev. Lett.*, *85*, 1020–1024.

Van Den Abeele, K. E.-A., P. A. Johnson, R. A. Guyer, and K. R. McCall (1997), On the analytical solution of hysteretic nonlinear response in elastic wave propagation, *J. Acoust. Soc. Am.*, *101*, 1885–1898.

Van Den Abeele, K. E.-A., J. Carmeliet, J. A. Ten Cate, and P. A. Johnson (2000a), Nonlinear Elastic Wave Spectroscopy (NEWS) techniques to discern material damage. Part I: Nonlinear Wave Modulation Spectroscopy (NWMS), *Res. NonDestructive Eval.*, *12*, 17–30.

Van Den Abeele, K. E.-A., J. Carmeliet, and P. A. Johnson (2000b), Nonlinear Elastic Wave Spectroscopy (NEWS) techniques to discern material damage. Part II: Single mode nonlinear resonance acoustic spectroscopy, *Res. NonDestructive Eval.*, *12*, 31–43.

Van Den Abeele, K. E.-A., J. Carmeliet, P. A. Johnson, and B. Zinszner (2002), The influence of water saturation on the nonlinear elastic mesoscopic response in earth materials and the implications to the mechanism of nonlinearity, *J. Geophys. Res.*, *107*(B6), 2121, doi:10.1029/2001JB000368.

Zinszner, B., P. A. Johnson, and P. N. J. Rasolofosaon (1997), Influence of change in physical state on elastic nonlinear response in rock: Effects of confining pressure and saturation, *J. Geophys. Res.*, *102*, 8105–8120.

F. Cohen-Tenoudji, Laboratoire Environnement et Developpement, Université Paris VII, 2 Place Jussieu, Paris 75251, France.

P. A. Johnson, Geophysics Group, Los Alamos National Laboratory, Mail Stop D443, Los Alamos, NM 87545, USA. (paj@lanl.gov)

P. Rasolofosaon, Rock Physics, Institut Français du Pétrole, Ave. Bois Preau, Rueil Malmaison, France. (patrick.rasolofosasoan@ifp.fr)

K. Van Den Abeele, Interdisciplinary Research Center, Faculty of Science, Catholic University Leuven Campus Kortrijk, E. Sabbelaan 53, B-8500 Kortrijk, Belgium. (koen.vandenabeele@kulak.ac.be)

B. Zinszner, Rock Physics, Institut Français du Pétrole, 2-4 Ave. Bois Preau, Rueil Malmaison, France. (bernard.zinszner@ifp.fr)